Influence of Native Ureolytic Microbial Community on Biocementation Potential of Sporosarcina Pasteurii

Raja Murugan
Indian Institute of Technology Madras
G. K. Suraishkumar
Indian Institute of Technology Madras
Abhijit Muhkerjee
Curtin University
Navdeep K Dhami (navdeep.dhami@curtin.edu.au)
Curtin University

Research Article

Keywords: Native Ureolytic Microbial Community, Biocementation Potential, Sporosarcina Pasteurii

Posted Date: July 9th, 2021

DOI: https://doi.org/10.21203/rs.3.rs-687770/v1

Influence of Native Ureolytic Microbial Community on Biocementation Potential of *Sporosarcina pasteurii*

Raja Murugan[1,2], G. K. Suraishkumar[1], Abhijit Muhkerjee[2], Navdeep K Dhami[2]

[1]Bhupat and Jyoti Mehta School of Biosciences, Indian Institute of Technology Madras, Chennai – 600036, India.

[2]School of Civil and Mechanical Engineering, Curtin University, Western Australia – 6102, Australia.

Correspondence and requests for material should be addressed to N.K.D. (email: navdeep.dhami@curtin.edu.au)

ABSTRACT

Microbially induced calcium carbonate precipitation (MICP)/Biocementation has emerged as a promising technique for soil engineering applications. There are chiefly two methods by which MICP is applied for field applications including biostimulation and bioaugmentation. Although bioaugmentation strategy using efficient ureolytic biocementing culture of *Sporosarcina pasteurii* is widely practiced, the impact of native ureolytic microbial communities (NUMC) on $CaCO_3$ mineralisation via *S. pasteurii* has not been explored. In this paper, we investigated the effect of different concentrations of NUMC on MICP kinetics and biomineral properties in the presence and absence of *S. pasteurii.* Kinetic analysis showed that the biocementation potential of *S. pasteurii* is 6-fold higher than the NUMC and is not significantly impacted even when the concentration of the NUMC is eight times higher. Micrographic results revealed a quick rate of $CaCO_3$ precipitation by *S. pasteurii* led to the generation of smaller $CaCO_3$ crystals (5 - 40 µm), while the slow rate of $CaCO_3$ precipitation by NUMC led to the creation of larger $CaCO_3$ crystals (35 - 100 µm). Mineralogical results

showed the predominance of the calcite phase in both sets. The outcome of the current study is crucial for tailor-made applications of MICP.

INTRODUCTION

Microbially induced calcium carbonate precipitation (MICP) is a ubiquitously recorded process in nature and is responsible for the creation of numerous geological formations in terrestrial and marine environments[1]. Recently this process has been replicated in the lab conditions for numerous engineering applications, as it leads to the formation of carbonate cement at ambient temperature conditions by harnessing the cementation potential of living microorganisms. The major applications include improvement of mechanical properties of soil[2,3], bioremediation of heavy metals and radio nucleotides[4-6], enhancement of oil recovery[7], repair of concrete cracks[8,9], and sequestration of atmospheric CO_2[10]. The chief benefit of this bio-mimicked cementation process includes self-healing ability, eco-friendliness, recyclability, and low viscosity paving the way for deeper penetration[11].

MICP/Biocementation occurs via various metabolic pathways of bacteria such as ureolysis, denitrification, sulfate reduction, and iron reduction[12]. Amongst the different pathways, MICP via ureolytic pathway is the most widely explored route because of its straightforwardness, efficacy, short time, and no excess production of protons[13,14]. In the microbial ureolytic pathway, urea is hydrolysed into ammonia and carbon dioxide by the action of urease[2]. Subsequently, these products equilibrate in water to form bicarbonate, ammonium, and hydroxide ions, which elevate the pH of the microenvironment around the bacteria (equation 1). An increase in pH favors the equilibrium shifts from bicarbonate ions to carbonate ions. The formed carbonate ions then precipitate as calcium carbonate on the bacterial surface in the presence of calcium[2] (equation 2).

$$\boldsymbol{Co(NH_2)_2 + 2\,H_2O \rightarrow HCO_3^{2-} + 2NH_4^+ + OH^-} \quad \textbf{(1)}$$

$$\boldsymbol{Ca^{2+} + CO_3^{2-} + bacteria \rightarrow bacteria - CaCO_3\downarrow} \quad \textbf{(2)}$$

For applications of MICP in soils, especially in the field, there are two modes by which calcifying bacteria are supplemented: biostimulation (enrichment of native population) or bioaugmentation (supplementation of efficient foreign bacteria). The biostimulation approach deals with the modification of existing field conditions by altering the nutrients, substrates, and electron acceptors to enrich the native microorganisms for accelerating the $CaCO_3$ precipitation; whereas, bioaugmentation includes the addition of highly potential ureolytic and cementing strains especially *Sporosarcina pasteurii* into the fields[32–36]. Comparing these two approaches, MICP through bioaugmentation has a major advantage as it is a rapid process. This benefit makes this approach quite attractive for engineering applications, despite having the limitation of cost factor for preparation and transport of bacterial cultures[35]. On the other hand, biostimulation utilizes native bacteria making the MICP process both economically and environmentally viable[35]. Furthermore, the stimulation approach may eliminate the possible ecological impacts caused by a non-indigenous bacterial introduction in the applied soil environment, but the process rate is generally slow in comparison to the bioaugmentation approach[37]. The studies conducted on utilisation of both the approaches for improving the soil engineering properties reported that changes in solution chemistry and distribution of $CaCO_3$ precipitate occurred invariably in 1-meter soil column during biostimulation[37]; however, bioaugmentation with *S. pasteurii* led to significant improvement in strength, stiffness, load-bearing capacity and hydraulic conductivity of the soil[12,37,38]. Although researchers have demonstrated biogeochemical changes during the biostimulation approach, not much has been investigated on the impact of native ureolytic microbial communities (NUMC) on the performance of *S. pasteurii* and how these communities perform in comparison to this high urease producing culture[37]. Also, the concentration of NUMC changes vastly in the field and may affect the kinetics of the $CaCO_3$ process, its mineralogy, and morphology which are the determining factors for the success of biocementation[22].

Kinetic aspects of the $CaCO_3$ precipitation decide the overall efficacy of biocementation and are influenced by both abiotic and biotic factors including temperature, pH, aeration, nutrient availability, bacterial concentration, and type of bacteria or type of microbial population[15–21]. Amongst all these factors, the concentration of bacteria and urease enzyme is a crucial factor[22] and is reflected in the kinetic constant of the $CaCO_3$ precipitation in terms of first-order rate constant of 0.002 to 0.60 h^{-1} [23–25]. Further, the kinetics of the process also control the morphological and nanomechanical properties of the precipitated $CaCO_3$; the slow rate of precipitation leads to the production of larger-sized crystals that are relatively stable compared to the smaller crystals formed at a high rate of precipitation[26,27].

In general, microbially induced $CaCO_3$ precipitate is a cohesive material[2] and exists in different crystalline phases including calcite, vaterite, aragonite, monohydrocalcite, and ikaite[1]. The sizes of these crystals vary from 5 – 100 μm along with variations in their nanomaterial properties [28–30]. Essential properties such as size, shape, stability, solubility, and hardness of the $CaCO_3$ crystals determine the efficacy of MICP in engineering applications. For example, the conservation of building materials required more stable calcite than metastable vaterite and larger rhombohedral crystals (100 – 150 μm) are more preferable in soil stabilization applications[31]. But very little information is available on these aspects including the impact of native communities on MICP kinetics with and without *S. pasteurii*, the effect of the concentration of native communities on MICP, and the influence of kinetic factors on morpho-mineralogical properties of carbonate crystals. All these factors are crucial in determining the efficacy of biocementation for field applications. The purpose of this study is to

1) evaluate the influence of native ureolytic microbial community (NUMC) at varying concentrations on biocementation kinetics 2) analyse the bioaugmentation potential of *S. pasteurii* in presence of different concentrations of native ureolytic microbial community and

3) investigate the effect of different cell concentrations of NUMC on morphological-mineralogical properties of *S. pasteurii* driven MICP.

We hypothesize that the outcome of this study will help to tailor MICP kinetics, morphology, mineralogy, and material properties of biomineralised crystals via both the stimulation and augmentation approach.

RESULTS

Influence of the native ureolytic microbial community on the kinetics of calcium carbonate precipitation

To investigate the influence of native ureolytic microbial community (NUMC) on calcium carbonate precipitation at varying concentrations (0, 0.1, 0.2, 0.4, 0.8, 1.6, and 3.2 OD), soluble calcium concentration in the cementation medium was monitored for up to 288 hours (at an interval of 12 hours). From fig. 1a it can be observed that the soluble calcium concentration decreased over time in all the groups with varying rates except group A to which no NUMC was added. The calcium concentration decreased to 50% from the initial value for group B at 96^{th} hour, for group C at 60^{th} hour, for group D at 48^{th} hour, for group E at 36^{th} hour, and group F and G at the 24^{th} hour. At the end of the process, the soluble calcium ions in all the sets were exhausted, except in set A.

Kinetic constants (K_{cal}) of $CaCO_3$ precipitation were used to further investigate the effect of various parameters on carbonate precipitation[36]. The monitored profiles were computationally fitted using equation (4) to calculate K_{cal} values (Fig 1a). Table 1 shows K_{cal} values at varying NUMC. The K_{cal} values of the fitted graphs increased from group A (0 h^{-1}) to group G (0.078 h^{-1}). Further, it was found that the K_{cal} values can be described by a Michelis-Menten (MM) type equation (3) where K_x is a constant value, X is the bacterial concentration, and $K_{cal,\,max}$ is the maximum kinetic constant for calcium carbonate precipitation. When K_x is equal to X, the

value of K_{cal} is equal to half of the $K_{cal,\,max}$. The observed values are K_x = 1 OD and $K_{cal,\,max}$ = 0.1 h^{-1} in this study. Fig. 1b shows MM type plot that relates K_{cal} and NUMC concentration.

$$K_{cal} = \frac{K_{cal,max}\,X}{K_x + X} \quad (3)$$

Fig. 1c shows the pH change over time in all the sets. In the cementation medium, pH was observed to be between 6.5 and 8.3 in all the groups throughout the process. It can be seen that the rate of pH change within the groups followed a similar trend except for the control group A.

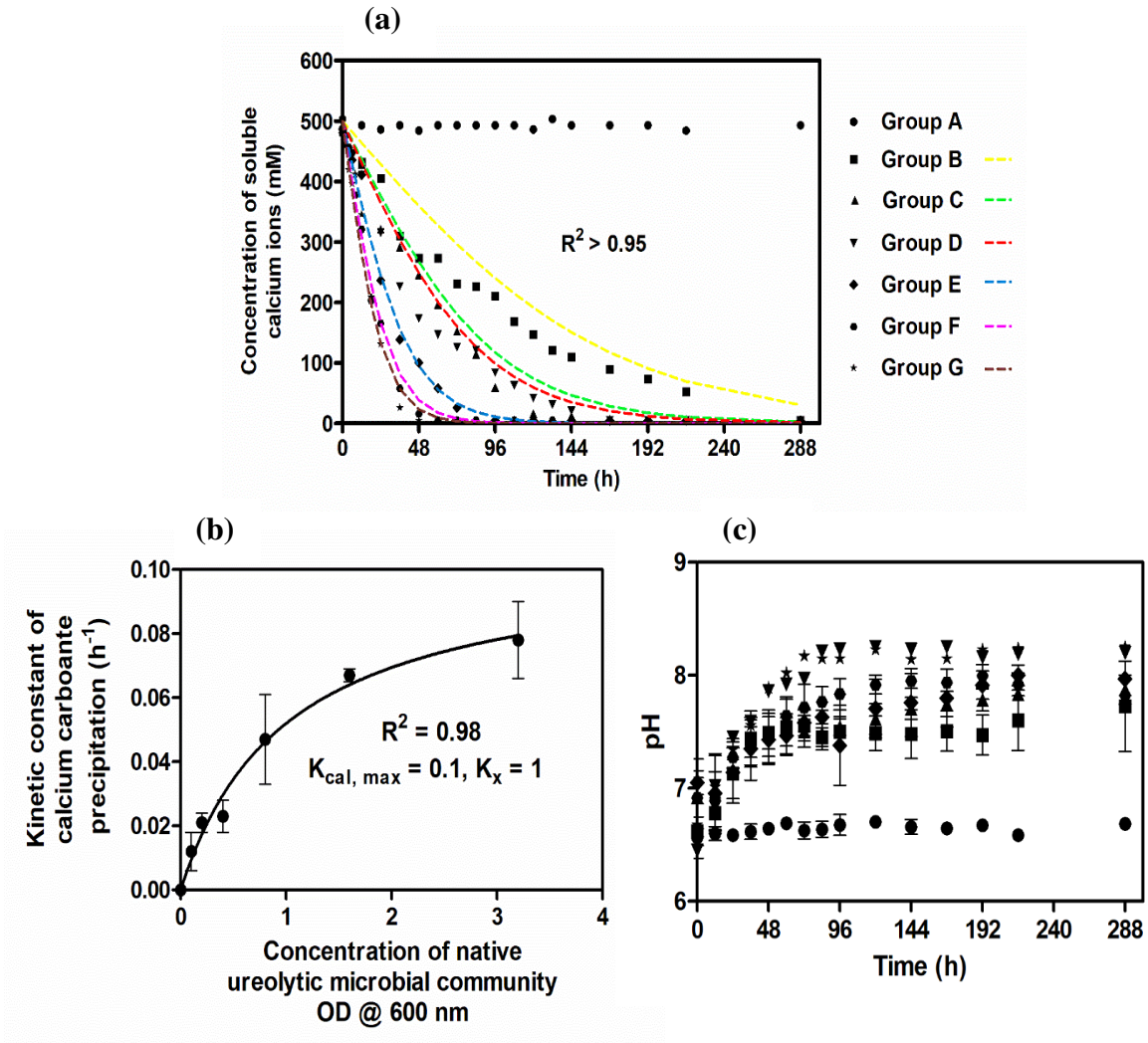

Figure 1. Concentration of soluble calcium ions over time (a). The relationship between the kinetic constant of $CaCO_3$ precipitation and concentration of the native ureolytic microbial community (b). The variation of pH with time (c). Group A – 0 OD NUMC, Group B – 0.1 OD NUMC, Group C – 0.2 OD NUMC, Group D – 0.4 OD NUMC, Group E – 0.8 OD NUMC, Group F – 1.6 OD NUMC, and Group G – 3.2 OD NUMC. NUMC – Native

Ureolytic Microbial Community. The coloured hidden lines are computationally fitted curves. Error bars in the figure indicate the standard deviation of three independent trials.

S. No	Native ureolytic microbial community Group ID	Concentration of NUMC OD @ 600 nm	Kinetic constant Of calcium carbonate precipitation (h^{-1})	R^2
1	Group A	0	0	NA
2	Group B	0.1	0.012 ± 0.006	0.97
3	Group C	0.2	0.021 ± 0.003	0.98
4	Group D	0.4	0.023 ± 0.005	0.98
5	Group E	0.8	0.047 ± 0.014	0.99
6	Group F	1.6	0.067 ± 0.002	0.99
7	Group G	3.2	0.078 ± 0.012	0.98

Table 1. The kinetic constant values of $CaCO_3$ precipitation at varying native ureolytic microbial community concentration. NUMC – Native Ureolytic Microbial Community. NA – Not Applicable. ± indicates the standard deviation of two independent trials.

Influence of the native ureolytic microbial community on augmented *S. pasteurii*

To investigate the influence of NUMC on *S. pasteurii* (bioaugmentation), soluble calcium concentration in the cementation medium was monitored over time and fitted with equation (4). Fig. 2a shows both observed and fitted curves from groups 1 to 7. From this figure, an exponential decrease of soluble calcium concentration was observed in all the groups with immediate effect upon the addition of NUMC and *S. pasteurii.* The concentration was recorded to be around zero at the 6^{th} hour. From the fitted curves, the values of the kinetic constants for calcium carbonate precipitation were calculated (Table 2) and compared (Fig. 2b). From Table 2 it can be seen that the kinetic constant values are 0.64, 0.65, 0.64, 0.73, 0.67, 0.66, 0.70, and 0.78 h^{-1} for the groups 1 to 7, respectively, i.e., the values were distributed between 0.64 and

0.78 h^{-1}. The change in the pH values of the cementation medium was also monitored (Fig. 2c) and the observed values were found to be between 6.5 and 8 for all the groups.

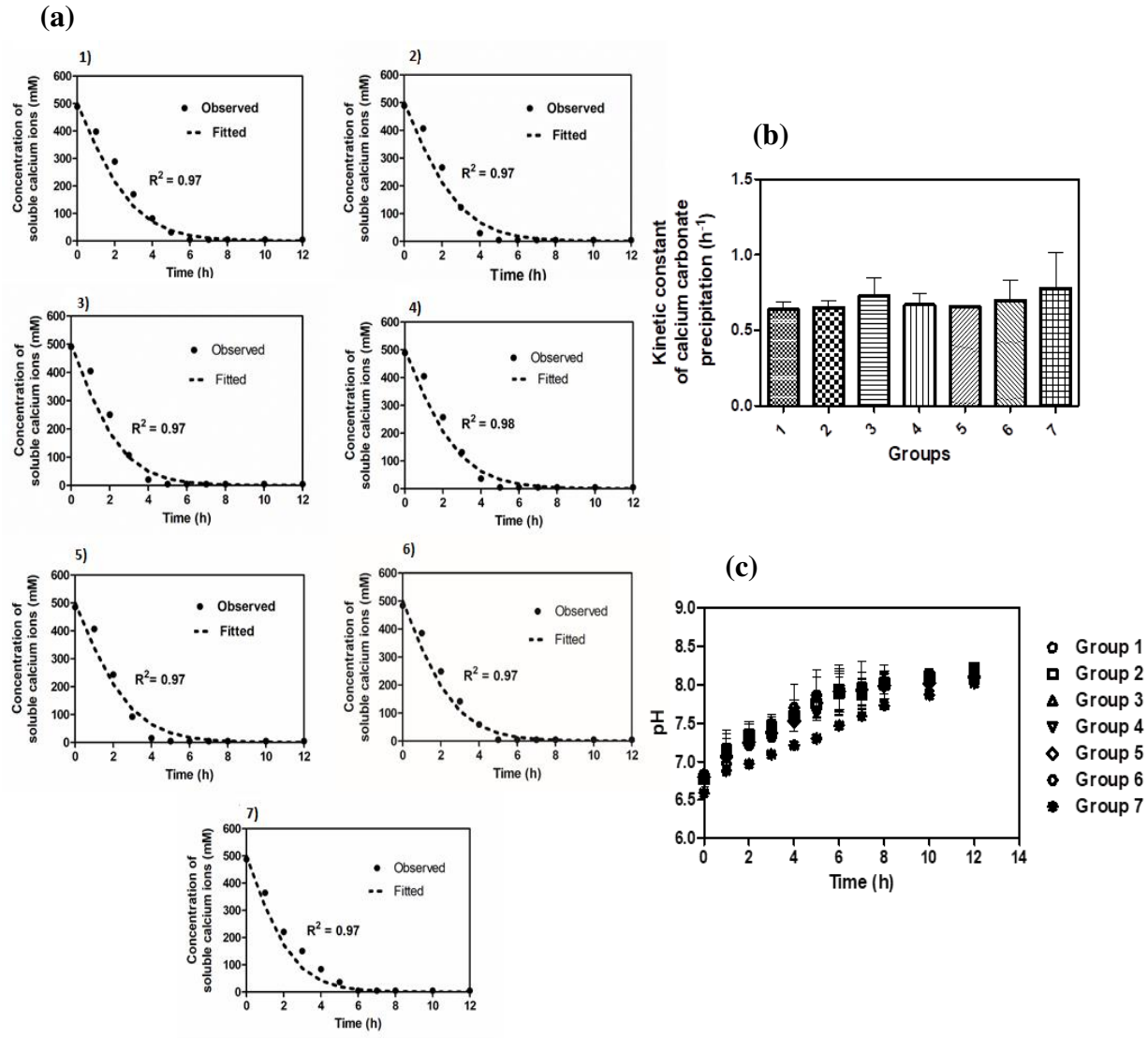

Figure 2. Concentration of soluble calcium ions over time - Bioaugmentation (a), comparison of the kinetic constant of $CaCO_3$ precipitation – Bioaugmentation (b), the variation of pH with time (c). Group 1 - 0 OD NUMC + 0.4 OD *S. pasteurii*, Group 2 - 0.1 OD NUMC + 0.4 OD *S. pasteurii*, Group 3 - 0.2 OD NUMC + 0.4 OD *S. pasteurii*, 4) Group 4 - 0.4 OD NUMC + 0.4 OD *S. pasteurii*, 0.8 OD NUMC + 0.4 OD *S. pasteurii*, 1.6 OD NUMC + 0.4 OD *S. pasteurii*, and 3.2 OD NUMC + 0.4 OD *S. pasteurii*. NUMC – Native Ureolytic Microbial Community. Bioaugmentation – (NUMC + *S. pasteurii*). Error bars in the figure 2b and 2c indicate the standard deviation of two independent trials.

S. No	Group ID	Concentration of NUMC OD @ 600 nm	Concentration of *S. pasteurii* OD@ 600 nm	Kinetic constant of $CaCO_3$ precipitation (h^{-1})	R^2
1	Group 1	0		0.64 ± 0.05	0.97
2	Group 2	0.1		0.65 ± 0.05	0.97

3	Group 3	0.2	0.4	0.73 ± 0.12	0.97
4	Group 4	0.4		0.67 ± 0.07	0.98
5	Group 5	0.8		0.66 ± 0.00	0.97
6	Group 6	1.6		0.70 ± 0.13	0.97
7	Group 7	3.2		0.78 ± 0.24	0.97

Table 2. The kinetic constants of calcium carbonate precipitation. ± indicates the standard deviation of two independent trials. NUMC – Native Ureolytic Microbial Community. *S. pasteurii – Sporosarcina pasteurii*.

Morphology and Phase of $CaCO_3$

$CaCO_3$ crystal morphology varies depending on the surface properties of the bacterial cell wall composition especially extracellular polymeric substances and the solution chemistry of the medium[26]. Hence, the shape and size of precipitated crystals were analysed via scanning electron micrography (Fig. 3). For groups 1 to 4, rhombohedral-shaped crystals of size 5 – 10 µm were observed for the samples collected at the 12^{th} hour. For group 5, the size of the individual and clustered rhombohedral-shaped crystals was found to be 15 – 25 µm for the samples collected at the 12^{th} hour. For groups 6 and 7, for the samples collected at the 12^{th} hour the size of both the clustered rhombohedral-shaped crystals was 30 – 40 µm. SEM images showed a cluster of rhombohedral-shaped crystals for the samples collected at 288^{th} hour for the groups B to G. The size of these crystals varied between 35 – 100 µm. The polymorph is a determining factor of strength and hardness of $CaCO_3$ in MICP. Therefore, the qualitative and quantitative information of the $CaCO_3$ crystals were obtained using the powdered XRD technique (for the groups B to G at 288^{th} hour and the groups 1 to 7 at the 12^{th} hour). Fig. 4 shows the XRD spectrum of group B and the representative spectrums of all the other groups. Tables 3 and 4 show the morphology and phase analysis of native ureolytic microbial community and bioaugmentation studies. It was observed that only group B showed 2.3 % of the vaterite phase of $CaCO_3$ crystals and all observed crystal phases of all the groups were of the calcite phase.

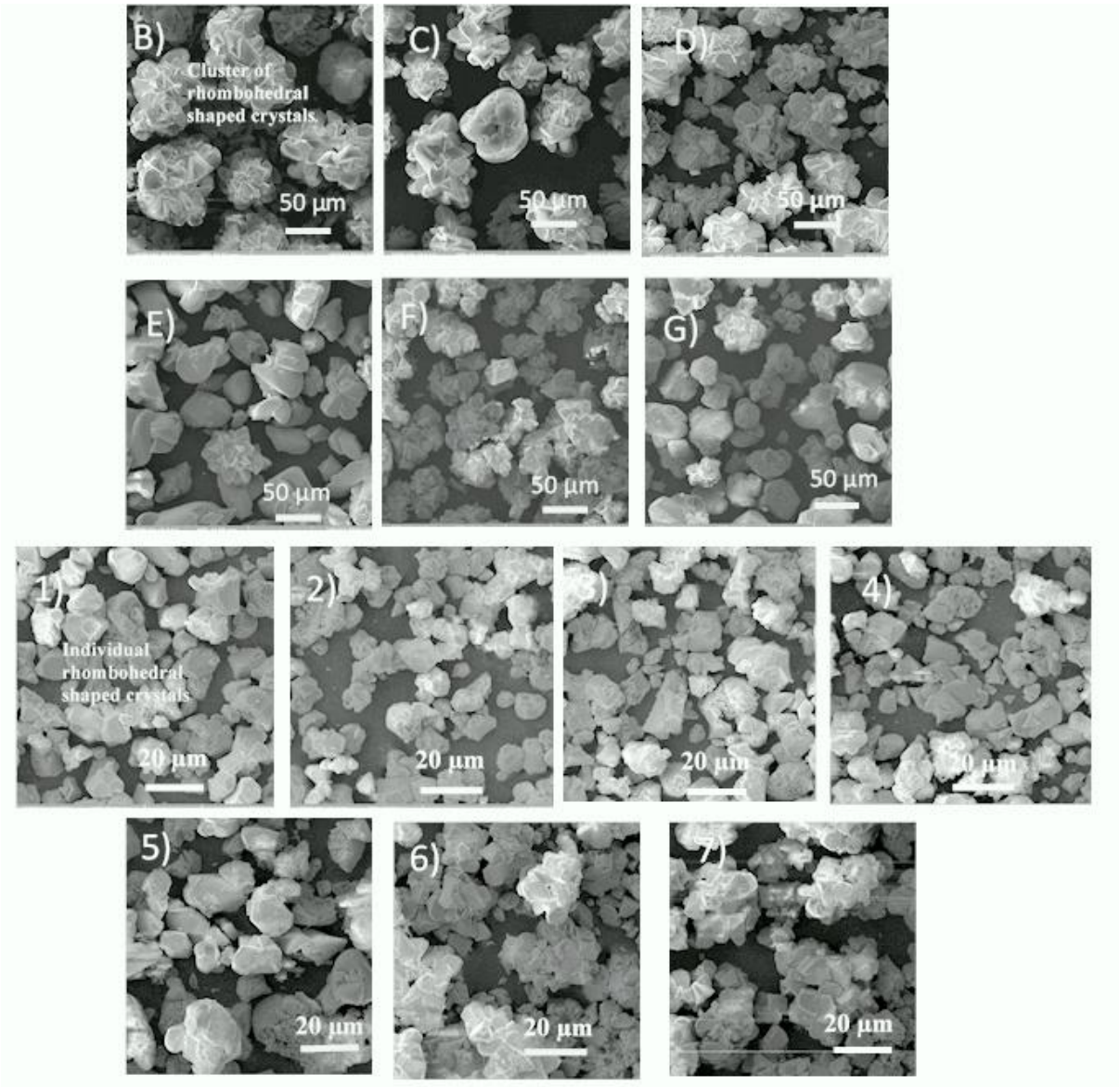

Figure 3. Scanning electron microscopy images of $CaCO_3$ crystals. Groups B to G (NUMC) and 1 to 7 (Bioaugmentation). B) – 0.1 OD NUMC, C) – 0.2 OD NUMC, D) – 0.4 OD NUMC, E) – 0.8 OD NUMC, F) – 1.6 OD NUMC, and G) – 3.2 OD. 1) - 0 OD NUMC + 0.4 OD *S. pasteurii*, 2) - 0.1 OD NUMC + 0.4 OD *S. pasteurii*, 3) - 0.2 OD NUMC + 0.4 OD *S. pasteurii*, 4) Group 4 - 0.4 OD NUMC + 0.4 OD *S. pasteurii*, 5) 0.8 OD NUMC + 0.4 OD *S. pasteurii*, 6) 1.6 OD NUMC + 0.4 OD *S. pasteurii*, and 7) 3.2 OD NUMC + 0.4 OD *S. pasteurii*. NUMC – Native Ureolytic Microbial Community and Bioaugmentation – (NUMC + *S. pasteurii*).

S. No	Group ID	Concentration of NUMC OD @ 600 nm	The average size of the crystal (µm)	Shape	Phase	
					Vaterite (%)	Calcite (%)
1	Group A	0	NA	NA	NA	NA
2	Group B	0.1	80 – 100	Cluster of rhombohedral	2.3	97.7
3	Group C	0.2	70 – 90	Cluster of rhombohedral	0	100
4	Group D	0.4	60 – 80	Cluster of rhombohedral	0	100

5	Group E	0.8	55 – 65	Individual and Cluster of rhombohedral	0	100
6	Group F	1.6	40 – 60	Individual and Cluster of rhombohedral	0	100
7	Group G	3.2	35 – 55	Individual and Cluster of rhombohedral	0	100

Table 3. The influence of native ureolytic microbial community concentration on the morphology and phase of $CaCO_3$ crystals. NUMC – Native Ureolytic Microbial Community. NA – Not Applicable.

S. No	Group ID	Concentration of NUMC OD @ 600 nm	Concentration of S. *pasteurii* OD@ 600 nm	The average size of the crystal (μm)	Shape	Phase
1	Group 1	0	0.4	5 – 10	Rhombohedral	Calcite
2	Group 2	0.1		5 – 10	Rhombohedral	
3	Group 3	0.2		5 – 10	Rhombohedral	
4	Group 4	0.4		5 – 10	Rhombohedral	
5	Group 5	0.8		15 – 25	Individual and cluster of rhombohedral	
6	Group 6	1.6		30 – 40	Cluster of rhombohedral	
7	Group 7	3.2		30 – 40	Cluster of rhombohedral	

Table 4. The morphology and phase characterization of $CaCO_3$ crystals - Bioaugmentation. NUMC – Native Ureolytic Microbial Community.

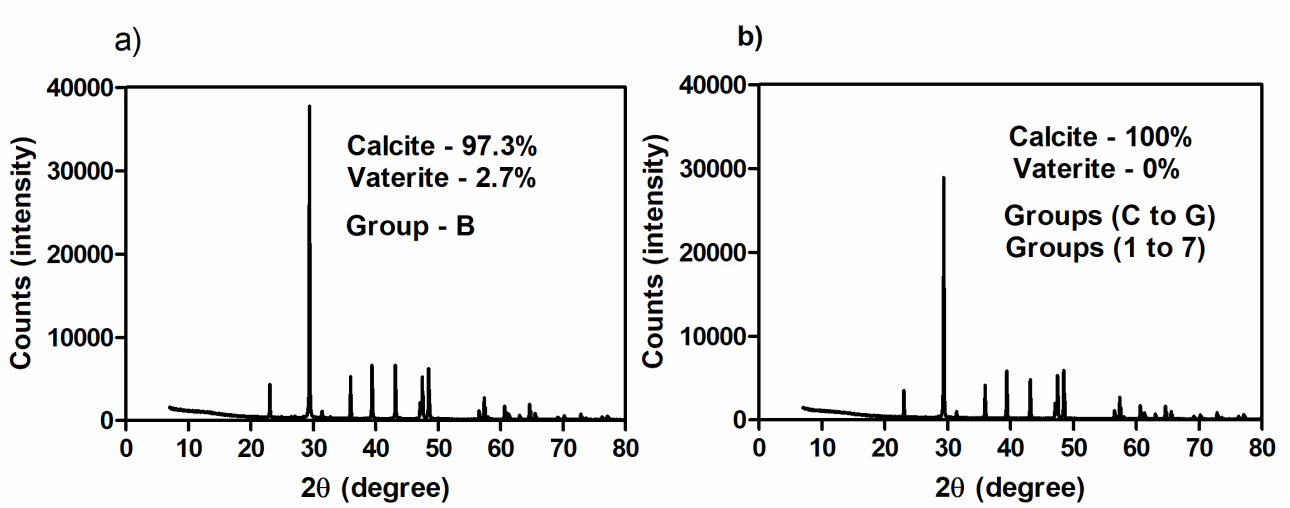

Figure 4. XRD spectrum of $CaCO_3$ polymorphs. a) Group B (NUMC) and b) Groups C to G (NUMC) and 1 to 7 (bioaugmentation). Group B – 0.1 OD NUMC, Group C – 0.2 OD NUMC, Group D – 0.4 OD NUMC, Group E – 0.8 OD NUMC, Group F – 1.6 OD NUMC, and Group G – 3.2 OD NUMC. Group 1 - 0 OD NUMC + 0.4 OD *S. pasteurii*, Group 2 - 0.1 OD NUMC + 0.4 OD *S. pasteurii*, Group 3 - 0.2 OD NUMC + 0.4 OD *S. pasteurii*, 4) Group 4 - 0.4 OD NUMC + 0.4 OD *S. pasteurii*, 0.8 OD NUMC + 0.4 OD *S. pasteurii*, 1.6 OD NUMC + 0.4 OD *S. pasteurii*, and 3.2 OD NUMC + 0.4 OD *S. pasteurii*. NUMC – Native Ureolytic Microbial Community, Bioaugmentation – (NUMC + *S. pasteurii*).

DISCUSSION

This study investigated the effect of NUMC on the augmented *S. pasteurii* by comparing the biocementing potentials of NUMC and augmented *S. pasteurii* in the presence of NUMC. To understand the effect, the kinetics of $CaCO_3$ precipitation, change in pH, the morphology of the $CaCO_3$ crystals formed and the phase of the precipitated crystals were analysed. The soluble calcium concentration was measured, and its kinetics was analysed using a logistic equation (4) to compare the biocementation potentials of NUMC and augmented *S. pasteurii* in the presence of NUMC. pH was also monitored to identify the range that favours $CaCO_3$ precipitation. SEM and XRD analyses were performed, which revealed the morphology (size and shape) and mineralogy of the crystals formed.

NUMC is capable of inducing $CaCO_3$ precipitation in their microenvironment[39]. In fig. 1a, the soluble calcium concentration decreased in all the groups. It could be due to carbonate ions generated in the MICP process during urea hydrolysis, which facilitates precipitation of soluble calcium around the bacterial cell wall in a cementation medium[2]. The complete exhaustion in the soluble calcium ions in the groups (group B – G) indicates that all the calcium in the medium is converted into $CaCO_3$. Moreover, the supplied equimolar concentration of urea is enough for the complete conversion of $CaCO_3$. The observed decrease in $CaCO_3$ precipitation rate (Fig. 1a) is due to encapsulation of $CaCO_3$ on the bacterial surface that limits the transport of nutrients transport including urea across the bacterial membrane[40]. The rate of soluble calcium depletion was observed to increase on increasing the NUMC concentration in the cementation medium. Increasing the NUMC concentration increases the total urease activity of the system, which in turn increases the soluble calcium depletion rate[22]. Moreover, the results show a positive correlation between $CaCO_3$ precipitation rate and the cell concentration [22–24]. Furthermore, the relationship between K_{cal} and NUMC concentration could be used to design and develop a similar process for field applications. The kinetic constant $K_{cal,\,Max}$ in the

mathematical equation 3 denotes the maximum ability of the NUMC to achieve MICP at a faster rate, in this case, 0.1 h^{-1}. The kinetic constant K_x is equal to 1 OD, which indicates the concentration of NUMC required to achieve half the value of $K_{cal, Max}$.

S. pasteurii is a widely employed bacterial strain for bioaugmentation of soil consolidation and stabilization process because of its high urease-producing potential[41]. Hence, this bacterium was chosen as the model organism for this study. Supersaturation Index (SI) is one of the key parameters for the initiation of $CaCO_3$ precipitation[32]. Quick $CaCO_3$ precipitation was observed for groups 1-7 in the cementation medium. This indicates that the cementation medium has reached the required SI in a short time. pH also affects the SI, which is evident from the reported result[42] (Fig. 2c). Moreover, the ready availability of the positively charged calcium ions in the vicinity of the negatively charged bacterial surface could also favour quick $CaCO_3$ precipitation[3].

The observed K_{cal} value of group 1 (0.64 h^{-1}) with *S. pasteurii* of 0.4 OD was 6-fold higher than the $K_{cal, Max}$ (0.1 h^{-1}) value of NUMC. This indicates that *S. pasteurii* has relatively high $CaCO_3$ precipitation potential compared to NUMC. However, the observed results are in contrast to the reported studies that suggest biostimulation is the best possible approach for biocementation[39,43]. This could be due to the presence of different NUMC and varying study conditions between different research groups. The influence of varying concentrations of NUMC on the bioaugmentation potential of *S. pasteurii* was also investigated. However, no significant changes in the K_{cal} values were observed within the groups when K_{cal} values were compared between groups 1 to 7 (Fig. 2b). This indicates that the presence of NUMC did not influence the $CaCO_3$ precipitation potential of *S. pasteurii* even at a concentration as high as 8-fold (group 7) over a period of two weeks in this study.

The pH of the cementation medium greatly influences the $CaCO_3$ precipitation and also affects bacterial urease production [42]. In this study, the pH of the cementation medium of all the groups

253 irrespective of the group type varied between 6.5 to 8.3. This indicates that the $CaCO_3$
254 precipitation occurred between the observed pH range. Urease activity of the bacteria results
255 in the generation of ammonium ions that in turn affects the pH of the cementation medium.
256 The rate of pH change was observed to be comparatively high for groups 1 to 7, which could
257 be attributed to the high urease activity of *S. pasteurii*[44]. However, the same was not observed
258 in groups A to G which could be attributed to the low urease activity of NUMC.
259 The molecular mechanism of $CaCO_3$ crystal nucleation, growth, and morphology (size and
260 shape) in the biocementation process is a complex phenomenon. Nature of the bacterial
261 community, solution chemistry of the cementation medium (supersaturation index), the
262 concentration of nutrients, calcium, and Mg^{2+} ions significantly influence the crystal growth
263 kinetics and characteristics[45,46,48]. In this study, groups B to G with only NUMC at different
264 concentrations showed a cluster of rhombohedral-shaped crystals, sized 35 -100 µm at 288th
265 hour. Whereas groups 1 to 4 with *S. pasteurii* in particular, yielded individual crystals of size
266 5 - 10 µm at 12th hour. A decrease in crystal size during bioaugmentation is due to the high
267 driving force, which results in the fast attaining of the saturation state during $CaCO_3$
268 precipitation. According to the classical nucleation theory: the nucleus size of the crystal
269 decreases when the driving force to reach the saturation state for the precipitation increases[47].
270 This result is consistent with a previous study by Cuthbert and co-workers who reported that a
271 higher initial saturation state influences the lower-sized crystals[40].
272 The generation of ammonium ions and inorganic carbon due to the effective urea hydrolysis
273 increases the pH and alkalinity of the cementation medium. It develops the oversaturated
274 cementation solution that leads to the spontaneous $CaCO_3$ precipitation[32]. It is possible to
275 obtain different phases of $CaCO_3$ including aragonite, calcite, vaterite, and two hydrated
276 crystalline phases as monohydric calcite and ikaite in the MICP process[1]. This is because the
277 polymorphism of $CaCO_3$ is highly dependent on various parameters of the precipitation

278 environment. In general, many studies reported that the phase transition from metastable
279 vaterite phase to more stable calcite phase during the $CaCO_3$ precipitation process[22,26]. But, the
280 specific phase preference by different bacterial cultures could depend on several parameters
281 including the type of bacteria, specific amino acid sequences of urease, organic acid
282 production, extracellular polymeric substances of the bacteria, the kinetics of the precipitation
283 process, cementation medium composition, and other physicochemical parameters that affect
284 supersaturation index of the solution [48-52].
285 In this study, no visible $CaCO_3$ crystals were observed in group A due to a lack of bacterial
286 metabolic activity that leads to the undersaturation of the system. In the case of group B, besides
287 97.7 % of calcite, 2.3 % of vaterite form of $CaCO_3$ crystals were formed at the end 288th hour.
288 On the other hand, in all other groups including group C to G and group 1 to 7 only calcite
289 form of $CaCO_3$ crystals was observed at the end of precipitation. From the results, it is evident
290 that calcite is the predominant polymorph of $CaCO_3$ crystals in both cases. It is also evident
291 that the presence of NUMC does not affect calcite formation. Moreover, the observed results
292 follow the Ostwald rule of crystallization, which states that thermodynamically crystal
293 formation favors the less soluble calcite than more soluble vaterite[27]. There could be a possible
294 delay in the transformation of vaterite to calcite form when the rate of $CaCO_3$ precipitation is
295 slow. Hence, this could be attributed to the slow transformation of vaterite to calcite in groups
296 B to G[27]. Nevertheless, only rhombohedral-shaped calcite form of crystals was observed in all
297 the groups despite different bacteria employed in this study at the end of the process. These
298 calcite form crystals have superior engineering properties (strength and stiffness) compared to
299 vaterite and aragonite forms of $CaCO_3$ crystals.

300 **Conclusions**

301 In this study, we investigated the influence of native ureolytic microbial communities (NUMC)
302 on the biocementation potential of the most widely used bacterial culture *Sporosarcina*

303 *pasteurii*. We evaluated the biogenic $CaCO_3$ precipitation kinetics of NUMC at varying
304 concentrations in the presence and absence of *S. pasteurii* along with its impact on the morpho-
305 mineralogical characteristics of the precipitated carbonates. Our key findings were that the
306 concentration of cells has a major impact on the reaction kinetics as well as morpho-
307 mineralogical properties of precipitated carbonate crystals as we recorded in the case of NUMC
308 as well as *S. pasteurii*. The rate of ureolysis and calcium carbonate precipitation in the case of
309 NUMC is very slow compared to *S. pasteurii*; and this can have a major impact on its
310 application. *S. pasteurii* is highly efficient in biocementation even in the presence of native
311 ureolytic cultures at different concentrations. Ureolytic and calcium carbonate precipitation
312 kinetics of *S. pasteurii* were not found to be impacted significantly in the presence of NUMC;
313 even when their concentration is eight folds higher. Although the rate of ureolysis and
314 carbonate precipitation is low in the case of NUMC, but it has a positive impact on the quality
315 of crystals. The size of calcite crystals in the case of NUMC with low metabolic activity is
316 much higher (6-10 times) compared to smaller crystals formed by *S. pasteurii*. This
317 demonstrates that depending upon the nature of application and time frame for cementation in
318 field-scale/ other areas, it is crucial to have the fundamental information on biocementation
319 potential of native communities and then look for alternatives as supplementation of *S.*
320 *pasteurii*. Taken together, the results from the current study demonstrate, for the first time, that
321 the quantitative and qualitative properties of biocement can be tailored utilising the information
322 of ureolytic and carbonate precipitation kinetics with native as well as augmented cultures. This
323 finding can enable several new possibilities for ureolysis driven biocementation in the area of
324 advanced functional living materials.

MATERIALS AND METHODS

Bacteria, Growth medium, and OD measurement

The bacteria used in this study are the Native Ureolytic Microbial Community (NUMC)[53] and *S. pasteurii (ATCC 11859)*. The bacteria were grown in Ammonium -Yeast extract medium (ATCC 1376) contains yeast extract (20 g/L), ammonium sulphate (10 g/L), and 0.13 M tris base (pH 9) were maintained at 30 ºC and 180 rpm. The individual components of the growth medium were autoclaved and mixed after cooling under sterile conditions. To measure the concentration of the overnight grown NUMC and *S. pasteurii,* the media containing bacteria were centrifuged at 4500 rpm for 10 minutes and the optical density was measured using a spectrophotometer (Thermo scientific, Genesis 10S) at 600 nm with 0.85 % sodium chloride solution as blank.

Cementation medium and conditions

The cementation medium provides required nutrients and cementation components for NUMC and *S. pasteurii*. 100 mL of cementation medium was prepared by mixing 65 mL of autoclaved distilled water containing 0.2 g of yeast extract followed by the addition of required concentrations of NUMC and *S. pasteurii* cell pellet obtained after centrifugation (4500 rpm for 10 minutes). Then 10 and 25 mL of filter-sterilized 5 M urea and 2 M calcium chloride dihydrate solution were added, respectively. The cementation medium containing a bacterial pellet was maintained at 30 ºC and 180 rpm in a shaker incubator.

Enumeration of bacterial concentration

The bacterial concentration was measured by the serial dilution method. Petri plates containing 1.5 % agar in ATCC 1376 media were used to spread the bacteria; 1 OD of bacteria in saline was found to contain cells equivalent to $4.5*10^8$ cells/mL.

Study design

This study was designed to investigate the influence of NUMC on the biocementation potential of augmented *S. pasteurii*. The study was divided into two major groups. Each group is further subdivided into seven subgroups namely A to G and 1 to 7. The groups A, B, C, D, E, F, and G have overnight grown NUMC pellet mixed with cementation medium at concentrations of 0, 0.1, 0.2, 0.4, 0.8, 1.6, and 3.2 OD, respectively. The groups 1, 2, 3, 4, 5, 6, and 7 contain fixed concentration of *S. pasteurii* (0.4 OD) and NUMC at concentrations of 0, 0.1, 0.2, 0.4, 0.8, 1.6, and 3.2 OD, respectively in the cementation medium. To monitor the process, 2 mL of samples were taken and centrifuged at 3000 rpm for 10 minutes at regular intervals of time. The obtained supernatant was used to measure soluble calcium concentration and pH until the process was complete.

Measurement of soluble calcium ions and pH

The soluble calcium ions were measured by using the complexometric titration procedure[54]. 40 µL of the sample was diluted to 10 mL followed by the addition of 400 µL 1 N sodium hydroxide solution and a few drops of hydroxy naphthol blue disodium salt (1% W/V) solution indicators. Then the mixture was titrated against 1 mM EDTA disodium salt solution until the colour change from pink to blue was observed. The slope of the standard (0 – 2.5 mM $CaCl_2$) was used to calculate the actual concentration of calcium ions in the sample. The change in pH during biocementation was recorded using a pH meter (Thermo scientific, Orion star, A211).

Morphology and phase analysis of $CaCO_3$

The $CaCO_3$ precipitate from the cementation medium was analysed at the end of the process. 30 mL of sample was taken was centrifuged at 4500 rpm for 10 minutes. The pellets obtained were washed twice with distilled water and dried at 37 ℃ overnight. Then the dried crystals were subjected to scanning electron microscopy and XRD.

Morphology (Size and Shape)

The variable pressure electron microscope (VP – SEM, Zeiss, EVO 40 -XVP, 2008) was used to observe the size and shape of the $CaCO_3$ precipitate. The samples were placed on carbon-aluminum tape and coated using a carbon evaporative coater (creissington, 2080C, 2011). The beam intensity and voltage were 8.0 and 10 kV, respectively with a working distance of around 15 mm. The secondary electron imaging was used to obtain scanning electron micrographs. The sizes of the crystals from the micrographs were obtained using IMAJEJ (1.8.0 172) software.

Phase

Bruker D8 advance diffractometer with Ni-filtered Cu Kα radiation (40 kV, 40 mA) over the range 7 – 120° 2θ, with a step size of 0.015° was used to collect the XRD data. The powdered $CaCO_3$ was resuspended in ethanol and deposited onto low-background holders. Further, the phase identification was done in Bruker EVA 5.2 using the Crystallography Open Database (COD) (http://www.crystallogrphy.net/). The phase quantification was done in Topas Academic 7 using the Rietveld method. Also, the crystal structures were identified from the COD.

Calculation of kinetic constants for calcium carbonate precipitation

In this study, the soluble calcium concentration over time was fitted with equation 4 using the solver function in Excel (2016 MSO) to calculate kinetic constants of $CaCO_3$ precipitation.

$$\boldsymbol{C_{cal}\,(t) = 2C_0 / \left(1 + e^{K_{cal}\,t}\right)} \quad (4)$$

Where, C_o = initial concentration of calcium (mM),

C_{cal} (t) = soluble calcium concentration (mM) at given time,

t = time (h) and,

K_{cal} = kinetic constant of calcium carbonate precipitation (h^{-1}).

References

1. Dhami, N. K., Reddy, M. S. & Mukherjee, M. S. Biomineralization of calcium carbonates and their engineered applications: A review. *Front. Microbiol.* **4**, 1–14 (2013).

2. Stocks-Fischer, S., Galinat, J. K. & Bang, S. S. Microbiological precipitation of $CaCO_3$. *Soil Biol. Biochem.* **31**, 1563–1571 (1999).

3. Dejong, J. T., Mortensen, B. M., Martinez, B. C. & Nelson, D. C. Bio-mediated soil improvement. *Ecol. Eng.* **36**, 197–210 (2010).

4. Ferris, F. G., Phoenix, V., Fujita, Y. & Smith, R. W. Kinetics of calcite precipitation induced by ureolytic bacteria at 10 to 20°C in artificial groundwater. *Geochim. Cosmochim. Acta* **68**, 1701–1710 (2004).

5. Fujita, Y., Grant Ferris, F., Daniel Lawson, R., Colwell, F. S. & Smith, R. W. Calcium carbonate precipitation by ureolytic subsurface bacteria. *Geomicrobiol. J.* **17**, 305–318 (2000)

6. Kumari, D., Qian, X. Y., Pan, X., Achal, V. & Li, Q. Microbially-induced Carbonate Precipitation for Immobilization of Toxic Metals. *Adv. Appl. Microbiol.* **94**, 79–108 (2016).

7. Wu, J., Wang, X. B., Wang, H. F. & Zeng, R. J. Microbially induced calcium carbonate precipitation driven by ureolysis to enhance oil recovery. *RSC Adv.* **7**, 37382–37391 (2017).

8. Ramachandran, S. K., Ramakrishnan, V. & Bang, S. S. Remediation of concrete using micro-organisms. *ACI Mater. J.* **98**, 3–9 (2001).

9. Van Tittelboom, K., De Belie, N., De Muynck, W. & Verstraete, W. Use of bacteria to repair cracks in concrete. *Cem. Concr. Res.* **40**, 157–166 (2010).

10. Mitchell, A. C., Dideriksen, K., Spangler, L. H., Cunningham, A. B. & Gerlach, R. Microbially enhanced carbon capture and storage by mineral-trapping and solubility-trapping. *Environ. Sci. Technol.* **44**, 5270–5276 (2010).

11. Phillips, A. J. *et al.* Engineered applications of ureolytic biomineralization: A review.

Biofouling **29**, 715–733 (2013).

12. Van Paassen, L. A., Ghose, R., van der Linden, T. J. M., van der Star, W. R. L. & van Loosdrecht, M. C. M. Quantifying Biomediated Ground Improvement by Ureolysis: Large-Scale Biogrout Experiment. *J. Geotech. Geoenvironmental Eng.* **136**, 1721–1728 (2010).

13. Whiffin, V. S., van Paassen, L. A. & Harkes, M. P. Microbial Carbonate Precipitation as a Soil Improvement Technique. *Geomicrobiol. J.* **24**, 417–423 (2007).

14. Zhang, J. L. *et al.* Screening of bacteria for self-healing of concrete cracks and optimization of the microbial calcium precipitation process. *Appl. Microbiol. Biotechnol.* **100**, 6661–6670 (2016).

15. Mortensen, B. M., Haber, M. J., DeJong, J. T., Caslake, L. F. & Nelson, D. C. Effects of environmental factors on microbial induced calcium carbonate precipitation. *J. Appl. Microbiol.* **111**, 338–349 (2011).

16. Martinez, B. C. *et al.* Experimental Optimization of Microbial-Induced Carbonate Precipitation for Soil Improvement. *J. Geotech. Geoenvironmental Eng*. **139**, 587-598 (2013).

17. Soon, N.W., Lee, L.M., Khun, T.C. & Ling, H.S. Factors Affecting Improvement in Engineering Properties of Residual Soil through Microbial-Induced Calcite Precipitation. *Artic. J. Geotech. Geoenvironmental Eng.* **140**, 04014006 (2014).

18. Zhao, Q. *et al.* Factors Affecting Improvement of Engineering Properties of MICP-Treated Soil Catalyzed by Bacteria and Urease. *J. Mater. Civ. Eng.* **26**, 04014094 (2014).

19. Oral, Ç. M. & Ercan, B. Influence of pH on morphology, size and polymorph of room temperature synthesized calcium carbonate particles. *Powder Technol.* **339**, 781–788 (2018).

20. Li, M., Wen, K., Li, Y. & Zhu, L. Impact of Oxygen Availability on Microbially Induced Calcite Precipitation (MICP) Treatment. *Geomicrobiol. J.* **35**, 15–22 (2018).

21. Peng, J. & Liu, Z. Influence of temperature on microbially induced calcium carbonate precipitation for soil treatment. *PLoS One* **14**, e0218396 (2019).

22. Wen, K., Li, Y., Amini, F. & Li, L. Impact of bacteria and urease concentration on precipitation kinetics and crystal morphology of calcium carbonate. *Acta Geotech.* **15**, 17–27 (2020).

23. Okwadha, G. D. O. & Li, J. Optimum conditions for microbial carbonate precipitation. *Chemosphere* **81**, 1143–1148 (2010).

24. Lauchnor, E. G., Topp, D. M., Parker, A. E. & Gerlach, R. Whole cell kinetics of ureolysis by Sporosarcina pasteurii. *J. Appl. Microbiol.* **118**, 1321–1332 (2015).

25. Mitchell, A. C. *et al.* Kinetics of calcite precipitation by ureolytic bacteria under aerobic and anaerobic conditions. *Biogeosciences* **16**, 2147–2161 (2019).

26. Heveran, C. M. *et al.* Engineered Ureolytic Microorganisms Can Tailor the Morphology and Nanomechanical Properties of Microbial-Precipitated Calcium Carbonate. *Sci. Rep.* **9**, 1–13 (2019).

27. Mitchell, A. C. & Grant Ferris, F. The influence of bacillus pasteurii on the nucleation and growth of calcium carbonate. *Geomicrobiol. J.* **23**, 213–226 (2006).

28. Hammes, F., Boon, N., De Villiers, J., Verstraete, W. & Siciliano, S. D. Strain-specific ureolytic microbial calcium carbonate precipitation. *Appl. Environ. Microbiol.* **69**, 4901–4909 (2003).

29. Rodriguez-Navarro, C., Jimenez-Lopez, C., Rodriguez-Navarro, A., Gonzalez-Muñoz, M. T. & Rodriguez-Gallego, M. Bacterially mediated mineralization of vaterite. *Geochim. Cosmochim. Acta* **71**, 1197–1213 (2007).

30. Chen, L. *et al.* Bacteria-mediated synthesis of metal carbonate minerals with unusual morphologies and structures. *Cryst. Growth Des.* **9**, 743–754 (2009).

31. Dhami, N. K., Mukherjee, A. & Reddy, M. S. Micrographical, mineralogical and nano-

471 mechanical characterisation of microbial carbonates from urease and carbonic anhydrase
472 producing bacteria. **94**, 443–454 (2016).
473 32. Fujita, Y., Grant Ferris, F., Daniel Lawson, R., Colwell, F. S. & Smith, R. W. Calcium
474 carbonate precipitation by ureolytic subsurface bacteria. *Geomicrobiol. J.* **17**, 305–318
475 (2000).
476 33. Burbank, M. B., Weaver, T. J., Green, T. L., Williams, B. & Crawford, R. L.
477 Precipitation of calcite by indigenous microorganisms to strengthen liquefiable soils.
478 *Geomicrobiol. J.* **28**, 301–312 (2011).
479 34. Gomez, M. G. *et al.* Field-scale bio-cementation tests to improve sands. *Proc. Inst. Civ.*
480 *Eng. Gr. Improv.* **168**, 206–216 (2015).
481 35. Gomez, M. G. *et al.* Large-Scale Comparison of Bioaugmentation and Biostimulation
482 Approaches for Biocementation of Sands. *J. Geotech. Geoenvironmental Eng.* **143**,
483 04016124 (2017).
484 36. Tobler, D. J. *et al.* Comparison of rates of ureolysis between Sporosarcina pasteurii and
485 an indigenous groundwater community under conditions required to precipitate large
486 volumes of calcite. *Geochim. Cosmochim. Acta* **75**, 3290–3301 (2011).
487 37. Gomez, M. G., Graddy, C. M. R., Dejong, J. T. & Nelson, D. C. Biogeochemical
488 Changes During Bio-cementation Mediated by Stimulated and Augmented Ureolytic
489 Microorganisms. *Sci. Rep.* 1–15 (2019).
490 38. Dhami, N. K., Alsubhi, W. R., Watkin, E. & Mukherjee, A. Bacterial community
491 dynamics and biocement formation during stimulation and augmentation: Implications for
492 soil consolidation. *Front. Microbiol.* **8**, 1267 (2017).
493 39. Raveh-Amit, H. & Tsesarsky, M. Biostimulation in desert soils for microbial-induced
494 calcite precipitation. *Appl. Sci.* **10**, 2905 (2020).
495 40. Cuthbert, M. O. *et al.* Controls on the rate of ureolysis and the morphology of carbonate

precipitated by S. Pasteurii biofilms and limits due to bacterial encapsulation. *Ecol. Eng.* **41**, 32–40 (2012).

41. Gomez, M. G., DeJong, J. T., Anderson, C. M., Nelson, D. C. & Graddy, C. M. Large-Scale Bio-Cementation Improvement of Sands. in *Geotechnical and Structural Engineering Congress 2016 - Proceedings of the Joint Geotechnical and Structural Engineering Congress 2016* 941–949 (American Society of Civil Engineers, 2016).

42. Hammes, F. & Verstraete, W. Key roles of pH and calcium metabolism in microbial carbonate precipitation. *Rev. Environ. Sci. Biotechnol.* (2002).

43. Gomez, M. G., Graddy, C. M. R., DeJong, J. T., Nelson, D. C. & Tsesarsky, M. Stimulation of Native Microorganisms for Biocementation in Samples Recovered from Field-Scale Treatment Depths. *J. Geotech. Geoenvironmental Eng.* **144**, 04017098 (2018).

44. Bachmeier, K. L., Williams, A. E., Warmington, J. R. & Bang, S. S. Urease activity in microbiologically-induced calcite precipitation. *J. Biotechnol.* **93**, 171–181 (2002).

45. Okyay, T. O. & Rodrigues, D. F. Optimized carbonate micro-particle production by Sporosarcina pasteurii using response surface methodology. *Ecol. Eng.* **62**, 168–174 (2014).

46. Chekroun, K. Ben *et al.* Precipitation and growth morphology of calcium carbonate induced by Myxococcus xanthus: Implications for recognition of bacterial carbonates. *J. Sediment. Res.* **74**, 868–876 (2004).

47. Oxtoby, D. W. Homogeneous nucleation: Theory and experiment. *J. Phys. Condens. Matter* **4**, 7627–7650 (1992).

48. Al Imran, M., Shinmura, M., Nakashima, K. & Kawasaki, S. Effects of Various Factors on Carbonate Particle Growth Using Ureolytic Bacteria. *Mater. Trans.* **59**, 1520–1527 (2018).

49. Lee, Y. S. & Park, W. Current challenges and future directions for bacterial self-healing

concrete. *Appl. Microbiol. Biotechnol.* **102**, 3059–3070 (2018).

50. Sondi, I. & Salopek-Sondi, B. Influence of the primary structure of enzymes on the formation of $CaCO_3$ polymorphs: A comparison of plant (Canavalia ensiformis) and bacterial (Bacillus pasteurii) ureases. *Langmuir* **21**, 8876–8882 (2005).

51. Rodriguez-Blanco, J. D., Shaw, S. & Benning, L. G. The kinetics and mechanisms of amorphous calcium carbonate (ACC) crystallization to calcite, via vaterite. *Nanoscale* **3**, 265–271 (2011).

52. Rodriguez-Navarro, C., Jroundi, F., Schiro, M., Ruiz-Agudo, E. & González-Muñoz, M. T. Influence of substrate mineralogy on bacterial mineralization of calcium carbonate: Implications for stone conservation. *Appl. Environ. Microbiol.* **78**, 4017–4029 (2012).

53.Dubey, A. et al. Biocementation mediated by stimulated ureolytic microbes from brahmaputra riverbank for mitigation of soil erosion. 26 February 2021, preprint (version 1) available at research square [https://doi.org/10.21203/rs.3.rs-235959/v1].

54. APHA/AWWA/WEF. Standard Methods for the Examination of Water and Wastewater. *Stand. Methods* 541 (2012).

Acknowledgments

The authors would like to acknowledge the Microscopy and Microanalysis Facility, Curtin University, Western Australia for SEM and XRD analysis. The current study was funded by the Australian Research Council Linkage Project LP180100132.

Authors Contributions

R.M. performed the experiments; R.M., N.K.D., G.K.S., and A.M. contributed to experimental design and data analysis; R.M., and N.K.D. wrote the manuscript. All the authors reviewed the manuscript.

Additional Information

Competing financial interests: The authors declare no competing financial interests.